



## OPEN ACCESS

## EDITED BY

Epaminondas Doxakis,  
Biomedical Research Foundation of the  
Academy of Athens (BRFAA), Greece

## REVIEWED BY

Sabine Levi,  
Institut National de la Santé et de la  
Recherche Médicale (INSERM), France  
Wolfgang B. Liedtke,  
Regeneron Pharmaceuticals, Inc.,  
United States

## \*CORRESPONDENCE

Anastasia Ludwig  
✉ anastasia.ludwig@helsinki.fi

<sup>†</sup>These authors have contributed equally to  
this work

RECEIVED 03 October 2024

ACCEPTED 10 December 2024

PUBLISHED 15 January 2025

## CITATION

Uvarov P, Fudo S, Karakus C, Golubtsov A,  
Rotondo F, Sukhanova T, Soni S, Di Scala C,  
Kajander T, Rivera C and Ludwig A (2025)  
Uncovering novel KCC2 regulatory motifs  
through a comprehensive transposon-based  
mutant library.  
*Front. Mol. Neurosci.* 17:1505722.  
doi: 10.3389/fnmol.2024.1505722

## COPYRIGHT

© 2025 Uvarov, Fudo, Karakus, Golubtsov,  
Rotondo, Sukhanova, Soni, Di Scala, Kajander,  
Rivera and Ludwig. This is an open-access  
article distributed under the terms of the  
[Creative Commons Attribution License  
\(CC BY\)](https://creativecommons.org/licenses/by/4.0/). The use, distribution or reproduction  
in other forums is permitted, provided the  
original author(s) and the copyright owner(s)  
are credited and that the original publication  
in this journal is cited, in accordance with  
accepted academic practice. No use,  
distribution or reproduction is permitted  
which does not comply with these terms.

# Uncovering novel KCC2 regulatory motifs through a comprehensive transposon-based mutant library

Pavel Uvarov<sup>1</sup>, Satoshi Fudo<sup>2†</sup>, Cem Karakus<sup>1†</sup>,  
Andrey Golubtsov<sup>1</sup>, Federico Rotondo<sup>1</sup>, Tatiana Sukhanova<sup>1</sup>,  
Shetal Soni<sup>1</sup>, Coralie Di Scala<sup>1,3</sup>, Tommi Kajander<sup>2</sup>,  
Claudio Rivera<sup>1,3</sup> and Anastasia Ludwig<sup>1\*</sup>

<sup>1</sup>Neuroscience Center, HiLIFE, University of Helsinki, Helsinki, Finland, <sup>2</sup>Institute of Biotechnology, HiLIFE, University of Helsinki, Helsinki, Finland, <sup>3</sup>INSERM, INMED, Aix Marseille University, Marseille, France

**Introduction:** The neuron-specific K-Cl cotransporter KCC2 maintains low intracellular chloride levels, which are crucial for fast GABAergic and glycinergic neurotransmission. KCC2 also plays a pivotal role in the development of excitatory glutamatergic neurotransmission by promoting dendritic spine maturation. The cytoplasmic C-terminal domain (KCC2-CTD) plays a critical regulatory role in the molecular mechanisms controlling the cotransporter activity through dimerization, phosphorylation, and protein interaction.

**Methods:** To identify novel CTD regulatory motifs, we used the Mu transposon-based mutagenesis system to generate a library of KCC2 mutants with 5 amino acid insertions randomly distributed within the KCC2-CTD. We determined the insertion positions in 288 mutants by restriction analysis and selected clones with a single insertion site outside known KCC2 regulatory motifs. We analyzed the subcellular distribution of KCC2-CTD mutants in cultured cortical neurons using immunocytochemistry and selected ten mutants with ectopic expression patterns for detailed characterization.

**Results:** A fluorescent Cl<sup>-</sup>-transport assay in HEK293 cells revealed mutants with both reduced and enhanced Cl<sup>-</sup>-extrusion activity, which overall correlated with their glycosylation patterns. Live-cell immunostaining analysis of plasma membrane expression of KCC2-CTD mutants in cultured cortical neurons corroborated the glycosylation data. Furthermore, the somatodendritic chloride gradient in neurons transfected with the KCC2-CTD mutants correlated with their Cl<sup>-</sup>-extrusion activity in HEK293 cells. Gain- and loss-of-function mutant positions were analyzed using available KCC2 cryo-EM structures.

**Discussion:** Two groups of mutants were identified based on 3D structural analysis. The first group, located near the interface of transmembrane and cytoplasmic domains, may affect interactions with the N-terminal inhibitory peptide regulating KCC2 activity. The second group, situated on the external surface of the cytoplasmic domain, may disrupt interactions with regulatory proteins. Analyzing CTD mutations that modulate KCC2 activity enhances our understanding of its function and is essential for developing novel anti-seizure therapies.

## KEYWORDS

KCC2, SLC12A5, GABA, chloride homeostasis, Mu transposon mutagenesis, KCC2-CTD mutations

## 1 Introduction

Neuron-specific K-Cl cotransporter KCC2 maintains low intracellular Cl<sup>-</sup> concentration ([Cl<sup>-</sup>]<sub>i</sub>) in neurons, rendering GABA<sub>A</sub> responses hyperpolarizing (Hübner et al., 2001; Rivera et al., 1999). KCC2 malfunction leads to compromised GABAergic inhibition, which may contribute to the onset of epileptic seizures (Barmashenko et al., 2011; Deeb et al., 2013; Pathak et al., 2007). Numerous mutations in the human KCC2 protein are associated with the development of epilepsy (Järvelä et al., 2024; Kahle et al., 2014; Puskarjov et al., 2014; Saito et al., 2017; Saitsu et al., 2016; Stöberg et al., 2015). Additionally, conditions such as brain tumors, ischemic stroke, and brain injuries are known to downregulate KCC2 expression, thereby increasing the likelihood of epileptic seizures (Bouleguez et al., 2010; Conti et al., 2011; Jarolimek et al., 1999; Khirug et al., 2005; Pallud et al., 2014; Sawant-Pokam et al., 2020). Preclinical research suggests that augmenting KCC2 activity could suppress seizures, highlighting the KCC2 role in modulating neuronal excitability under normal and epileptogenic conditions (Jarvis et al., 2023; Lee et al., 2021; Moore et al., 2018).

KCC2 C-terminal domain (CTD) is crucial for regulating KCC2 functionality. It harbors multiple regulatory phosphorylation sites, including Y903, T906, S932, T934, S937, S940, T1007, T1009, S1034, and Y1087, which modulate activity and membrane trafficking of the cotransporter (Cordshagen et al., 2018; Lee et al., 2007; Rinehart et al., 2009; Weber et al., 2014). In addition, the KCC2-CTD bears a calpain cleavage site that mediates activity-dependent degradation of KCC2 (Puskarjov et al., 2012; Wan et al., 2018; Zhou et al., 2012) and a non-canonical dileucine motif that controls KCC2 endocytosis (Zhao et al., 2008). In addition, a short CTD sequence called ISO domain mediates constitutive activity of KCC2 under isotonic conditions (Acton et al., 2012; Mercado et al., 2006). Finally, actin cytoskeleton regulatory proteins such as 4.1 N and β-PIX bind to the KCC2-CTD, and through this interaction, influence the shape of dendritic spines and the plasticity of glutamatergic synapses (Li et al., 2007; Llano et al., 2015).

In this study, we report the generation and analysis of a mutant library targeting KCC2-CTD. We utilized the Mu transposon-based mutagenesis system to create 288 mutants with 5 amino acid random insertion sites within KCC2-CTD. Based on immunocytochemical analysis, we selected ten mutants displaying expression patterns distinct from the wild-type (WT) KCC2. Among selected clones, a fluorescent Cl<sup>-</sup>-transport assay conducted in HEK293 cells revealed mutants exhibiting both reduced and enhanced Cl<sup>-</sup>-extrusion activity. The somatodendritic chloride gradient, measured using a patch clamp in cultured neurons transfected with the KCC2-CTD mutants, supported the results of the Cl<sup>-</sup>-transport assay in HEK293. Notably, high KCC2 membrane expression and mature glycosylation pattern of certain mutants did not necessarily guarantee their high K-Cl cotransport activity.

Given the diverse regulatory functions of CTD, our insertion CTD library promotes identification of novel motifs modulating various aspects of KCC2 activity. Through systematic analysis of the positions of the CTD mutations, we can gain valuable insights into the mechanisms governing KCC2 regulation and potentially

discover new targets for therapeutic intervention in neurological disorders.

## 2 Materials and methods

### 2.1 DNA constructs

As a template for the Entranceposon (M1-Kan) integration, we used the rat KCC2b ORF sequence containing one copy of FLAG-tag (DYKDDDDK) in the large 3rd extracellular loop and controlled by the CMV promoter (pCMV-KCC2\_FLAG-out) (Pressey et al., 2017). The extracellular FLAG-tag was inserted into the low-conserved region of the 3rd extracellular loop between amino acid positions 383 and 384 of the rat KCC2b. The insertion site is located in the loop away from the ECD secondary structures and from the previously described glycosylation sites. KCC2\_FLAG-out construct was previously characterized (Pressey et al., 2017) and found to be fully functional. pCAG-mGFP was a kind gift from Dr. Connie Cepko (Addgene plasmid #14757). pcDNA3.1(-) was used for mock transfections.

### 2.2 KCC2-CTD mutant library

The mutant library was generated using the commercially available transposition kit (Mutation Generation System Kit, catalog number F701, ThermoFisher Scientific) according to the manufacturer's instructions. The Entranceposon (M1-Kan) integration reaction was optimized to ensure that most of the mutants contained only one integration site. Kanamycin resistance gene within the transposon cassette was used to select the mutant clones. To restrict the mutagenesis exclusively to the distal C-terminal regulatory part (809–1,116 aa) of the large KCC2-CTD (635–1,116 aa), the mutant DNA plasmid library was cut at the unique *Bst*EII and *Afl*II restriction sites embracing the indicated regulatory region and ~300 bp of the proximal 3' untranslated region (3'UTR). The *Bst*EII-*Afl*II digestion products were gel-purified and ligated into the original unmutated KCC2 cDNA construct pre-cut similarly at *Bst*EII and *Afl*II sites. As a result, the final KCC2-CTD library contained mutations exclusively within the indicated KCC2b cDNA region. The transposon insertion cassette carrying the Kan-resistance gene, flanked by two *Not*I sites, was removed by *Not*I digestion and sticky-end re-ligation, thus leaving 15 bp fragments containing a single *Not*I site. High-efficiency NEB 5α competent cells (New England Biolabs) were transformed by the resultant KCC2-CTD library, and 288 bacterial colonies (3 × 96-well plates) were subjected to subsequent analysis.

### 2.3 Immunocytochemical analysis of KCC2 mutants in rat cultures

Rat cortical neurons were plated in a 96-well plate according to the protocol described previously (Ludwig et al., 2011). The cultures were transfected on day *in vitro* (DIV) 10 with a mixture of pCAG-mGFP and either pCMV-KCC2\_FLAG-out or FLAG-KCC2-CTD mutants using Lipofectamine 2000 transfection reagent (ThermoFisher Scientific) according to the manufacturer's protocol. Forty-eight hours

after transfection, cultures were washed twice with 1x PBS and fixed in 4% PFA (50  $\mu$ L/well) for 10 min, permeabilized with 0.1% Triton X-100 in 1x PBS for 5 min, and blocked in 10% normal donkey serum for 1 h. To study the intracellular distribution of the FLAG-KCC2-CTD mutants, the permeabilized cultures were incubated overnight with the mouse monoclonal anti-FLAG antibody (F3165, Sigma-Aldrich, 1:750). The next day, cultures were washed 3 times 20 min in 1x PBS and incubated with anti-mouse Cy5 (Jackson ImmunoResearch Laboratories, 1:400) secondary antibodies for 1 h at 37°C. DAPI was used to counterstain nuclei.

## 2.4 Immunocytochemical analysis of surface expression of KCC2 mutants in rat neurons

Rat cortical neurons were cultured on glass coverslips pretreated with poly-L-lysine as described previously (Ludwig et al., 2011). The cultures were transfected on DIV 6 with a mixture of mGFP and either wild-type or mutant KCC2\_FLAG-out constructs using Lipofectamine 2000 transfection reagent (ThermoFisher Scientific) according to the manufacturer's protocol. Two weeks after plating, transfected neurons were subjected to the surface immunolabeling protocol that comprises two steps. First step: Cultures were incubated with mouse anti-FLAG antibody (F3165, Sigma-Aldrich) diluted 1:200 in cell-culture medium for 30 min at 37°C, 5% CO<sub>2</sub>. The temperature and duration of the membrane KCC2 labeling step is the result of optimization by several groups working in the KCC2 field: 1 h at 37°C (Acton et al., 2012), 1.5 h at 37°C (Pressey et al., 2017), 2 h at 37°C (Friedel et al., 2017), and 1 h at 37°C (Järvelä et al., 2024). We found previously that lower temperatures resulted in a low labeling efficiency. After the incubation, cells were washed 3 times with ice-cold incubation buffer (NaCl, 127 mM; KCl, 3 mM, CaCl<sub>2</sub>, 2 mM; MgCl<sub>2</sub>, 1.3 mM; glucose, 20 mM; HEPES, 20 mM; pH 7.4) and incubated with anti-mouse Alexa Fluor 568 secondary antibody (Thermo Fisher Scientific) diluted 1:400 in the incubation buffer for 30 min at 13°C. This step reveals plasma membrane KCC2 immunoreactivity. Second step: Cells were washed 3 times with ice-cold incubation buffer and fixed with 4% PFA for 10 min at room temperature. After the fixation cells were washed 3 times with PBS, permeabilized with 0.1% TritonX-100 in PBS (TritonX/PBS), and the background signal was blocked with 10% goat serum in TritonX/PBS for 30 min at room temperature. After the blocking, cells were incubated with mouse anti-FLAG antibody (F3165, Sigma-Aldrich) diluted 1:400 in TritonX/PBS overnight at 4°C. Then cells were washed 3 times with TritonX/PBS and incubated with anti-mouse Alexa Fluor 647 secondary antibody (Thermo Fisher Scientific) diluted 1:400 in TritonX/PBS for 1 h at room temperature. After incubation with the secondary antibody, coverslips were washed once with TritonX/PBS, once with PBS, and once with distilled H<sub>2</sub>O, and mounted with Fluoromount-G (Southern Biotechnology). The second step reveals total KCC2 immunoreactivity.

## 2.5 Fluorescent Cl<sup>-</sup> extrusion assay and analysis

For Cl<sup>-</sup> extrusion assay HEK293T cells were cultured in Dulbecco's modified Eagle's medium supplemented with 10% fetal

bovine serum and penicillin/streptomycin antibiotic mix. The cells were cotransfected with SuperClomeleon (Grimley et al., 2013) and KCC2-CTD mutants using Lipofectamine 2000 according to the manufacturer's protocol. Cl<sup>-</sup> efflux assay was performed 40–44 h after transfection using a protocol described previously (Friedel et al., 2013) with some modifications. Briefly, HEK293 cells were pre-incubated in the extracellular solution (ECS: 140 mM NaCl, 2.5 mM KCl, 10 mM HEPES, 20 mM D-glucose, 2 mM CaCl<sub>2</sub>, 2 mM MgCl<sub>2</sub>, pH 7.4, 300 mOsm). Next, cells were loaded with Cl<sup>-</sup> by incubation for 10 min in 60  $\mu$ L of the loading solution with high [K<sup>+</sup>]<sub>o</sub> and high [Cl<sup>-</sup>]<sub>o</sub> (75 K<sup>+</sup>, 65 mM NaCl, 75 mM KCl, 10 mM HEPES, 20 mM D-glucose, 2 mM CaCl<sub>2</sub>, 2 mM MgCl<sub>2</sub>, pH 7.4, 300 mOsm). The high [K<sup>+</sup>]<sub>o</sub> rendered the membrane potential at the level sufficient for Cl<sup>-</sup> loading into HEK293 cells via endogenous Cl<sup>-</sup> channels and transporters. Previously we showed that raising the extracellular [K<sup>+</sup>]<sub>o</sub> up to 50 mM results in efficient Cl<sup>-</sup> loading even in the absence of GlyR- $\alpha$ 1 glycine receptors and glycine (Ludwig et al., 2017). Subsequent addition of 300  $\mu$ L of the K<sup>+</sup>-free solution (140 mM NaCl, 10 mM HEPES, 20 mM D-glucose, 2 mM CaCl<sub>2</sub>, 2 mM MgCl<sub>2</sub>, pH 7.4, 300 mOsm) was used to decrease [K<sup>+</sup>]<sub>o</sub>, thus initiating the KCC2-mediated Cl<sup>-</sup> extrusion in the resultant extrusion solution (127.5 mM NaCl, 12.5 mM KCl, 10 mM HEPES, 20 mM D-glucose, 2 mM CaCl<sub>2</sub>, 2 mM MgCl<sub>2</sub>, pH 7.4, 300 mOsm). VU0463271 (VU) stock solution was prepared in DMSO (30 mM), stored at -20°C, and used within a week. All solutions containing working concentrations of VU (30  $\mu$ M) were prepared freshly 1–2 h before the Cl<sup>-</sup> efflux assay.

Cl<sup>-</sup>-sensitive (YFP) and Cl<sup>-</sup>-insensitive (Cerulean) components of SuperClomeleon fluorescence were detected sequentially using the microplate reader (FLUOstar Optima FL, BMG Labtech) equipped with the filter sets for YFP (excitation 500 nm, emission 560 nm) and Cerulean (excitation 450 nm, emission 480 nm). F<sub>480</sub>/F<sub>560</sub> ratio, which directly correlates with the [Cl<sup>-</sup>]<sub>i</sub>, was recorded every 100 s during the loading (10 min) and extrusion (50 min) steps for VU+ and VU- wells corresponding to the same KCC2-CTD mutant. F<sub>480</sub> and F<sub>560</sub> background levels were measured in neighbor wells containing non-transfected HEK293 cells and were subtracted from the corresponding F<sub>480</sub> and F<sub>560</sub> values measured for the KCC2-CTD mutants. Analysis was performed using a custom-made Python script.

## 2.6 E<sub>GABA</sub> gradient-based Cl<sup>-</sup> extrusion assay

The assay of neuronal Cl<sup>-</sup> extrusion is based on imposing a somatic chloride load through a whole-cell patch-clamp electrode and measuring the somatodendritic gradient of the reversal potential of GABA<sub>A</sub> receptor-mediated current responses (E<sub>GABA</sub>) induced along the dendrite by local iontophoretic application of GABA. Somatic recordings in immature cultured hippocampal neurons (DIV 3) were performed in standard extracellular solution at 34°C in the whole-cell voltage-clamp configuration using an EPC 10 patch-clamp amplifier (HEKA Elektronik, Inc., Germany). The composition of the extracellular solution was (in mM): 127 NaCl, 3 KCl, 2 CaCl<sub>2</sub>, 1.3 MgCl<sub>2</sub>, 10 D-glucose, and 20 HEPES, pH 7.4 was adjusted with NaOH. Patch pipettes were fabricated from borosilicate glass (Harvard Apparatus, USA), and their resistances ranged from 6.5 to 8.5 M $\Omega$ . The composition of the patch pipette solution was (in mM): 29 KCl, 111 K-gluconate, 0.5 CaCl<sub>2</sub>, 2 NaOH, 10 D-glucose, 10 HEPES, and 2 Mg-ATP, 5 BAPTA, pH 7.3 was adjusted with KOH. For

local iontophoretic application of GABA, brief 100 ms positive current pulses (50–70 nA) were delivered by a sharp micropipette (40–45 M $\Omega$  when filled with 250 mM GABA in 250 mM HCl). Iontophoretic GABA injections were given no more than once per minute. A constant negative current of –5 nA was applied to the micropipette to compensate for the passive leak of GABA. GABA was applied at the soma and the dendrite (~30  $\mu$ m from the soma) of a given neuron. Membrane potential was clamped at –60 mV. All membrane potential values were corrected for a liquid-junction potential of 14.16 mV. Before recording, the first 2 min were dedicated to loading the whole cell with the intracellular solution. The reversal potential of GABAergic currents ( $E_{\text{GABA}}$ ) was determined from the current–voltage (I–V) relation obtained using ramp voltage protocol. NKCC1 was blocked throughout the experiments with 10  $\mu$ M bumetanide, action potentials with 1  $\mu$ M TTX, and GABA<sub>B</sub> receptors with 1  $\mu$ M CGP 35348 (Abcam). Under these conditions, the somatodendritic gradient  $\Delta E_{\text{GABA}}$  provides a quantitative estimate of the efficacy of KCC2-mediated Cl<sup>–</sup> extrusion.

## 2.7 Glycosylation analysis of KCC2-CTD mutants in HEK293 cells

Except for deglycosylation experiments, samples were prepared as described before (Uvarov et al., 2009), with small modifications. Briefly, HEK293T cells cultured in Dulbecco's modified Eagle's medium supplemented with 10% fetal bovine serum were transfected with 1  $\mu$ g of each plasmid carrying a KCC2 mutant gene using 3  $\mu$ g of polyethylenimine (PEI) and incubated for 48 h. For SDS-PAGE analysis without deglycosylation treatment, the cell samples were homogenized on ice in lysis buffer (50 mM Tris–HCl, 150 mM NaCl, 1% Triton X-100, 0.5% deoxycholic acid, 0.1% SDS, pH 8.0) supplemented with the Pierce protease inhibitor mini tablets, EDTA-free (Thermo Fisher). For SDS-PAGE analysis with deglycosylation treatment, the cell samples were lysed on ice in TNE buffer (1% Nonidet P-40, 50 mM Tris–HCl, 140 mM NaCl, 5 mM EDTA, pH 8.0), supplemented with the Pierce protease inhibitor mini tablets, EDTA-free (ThermoFisher) and 100  $\mu$ M iodoacetamide (Sigma). After centrifugation for 10 min (15,000  $\times$  g) at 4°C, protein concentrations of the supernatants were determined by using Pierce BCA protein assay kit (ThermoFisher).

The supernatants of HEK293 cell lysates containing KCC2 mutant proteins in TNE buffer were treated with PNGase F (New England Biolabs) and Endo H (New England Biolabs) according to manufacturer's instructions with a slight modification. Briefly, each sample was mixed with Glycoprotein Denaturing Buffer and heated at 60°C for 20 min. For PNGase F reaction, the sample was then mixed with GlycoBuffer 2, Nonidet P-40 (final 1%), and PNGase F and incubated at 37°C for 1 h. For Endo H reaction, the sample was mixed with GlycoBuffer 3 and Endo H and incubated at 37°C for 1 h. For negative controls, a duplicate was made for each sample following the same procedure except that PNGase F or Endo H was not added to the duplicate. The resultant reactions were analyzed by SDS-PAGE.

## 2.8 SDS-PAGE and Western blotting

Each sample containing 30  $\mu$ g protein was mixed with 5 $\times$  Laemmli loading buffer (300 mM Tris–HCl, 10% SDS, 50% glycerol,

0.05% bromophenol blue, pH 6.8) and DTT (final 70 mM). The lysates were not heated before loading on the SDS-PAGE. The protein samples were separated using 7.5% Mini-PROTEAN TGX precast protein gels (Bio-Rad) at 150 V for 60 min and then transferred onto PVDF membrane with Trans-Blot Turbo Transfer System (Bio-Rad).

Blots were blocked with 5% skim milk in Tris-buffered saline with 0.1% Tween 20 and probed with rabbit anti-KCC2 antibody (Millipore, 1:2500 dilution) and subsequently with horseradish peroxidase-conjugated goat anti-mouse IgG antibody (Santa Cruz). Blots were developed with Amersham ECL Prime Western Blotting reagents (Merck), visualized with ChemiDoc XRS+ (Bio-Rad), and analyzed with Image Lab software (Bio-Rad). All measurements were within the linear range of camera sensitivity.

## 3 Results

### 3.1 Generation of the KCC2-CTD mutant library and mapping the mutations

To identify regulatory motifs in the KCC2 C-terminal domain (CTD), we generated a library of the full-length KCC2b mutants containing bacteriophage Mu-mediated random insertions of 15 bp nucleotide sequence into the KCC2b cDNA part encoding the distal C-terminal domain between amino acids 809 and 1,116 (Figure 1A). This mutagenesis strategy resulted in 5-aa in-frame insertions within the distal CTD. The exact amino acid sequence of the insertions depended on the nucleotide sequence surrounding the insertion site. When inserted into the open reading frame of a protein, the transposon sequence ensured the absence of premature stop codons within the mutated region.

To map the positions of the insertions in the KCC2-CTD library, we purified 288 plasmids corresponding to the individual mutants and cut them with restriction enzymes *Bam*HI (located 489 bp upstream of the mutated CTD region) and *Not*I (at the insertion site) (Figure 1B). The *Bam*HI - *Not*I restriction products ranged between ~500 and ~1700 bp (Figure 1C), with a total of 288 mutations spread across the mutated region, including 221 located between 809 and 1,116 aa of KCC2-CTD and 67 in the 300 bp fragment of the KCC2 proximal 3'UTR. In agreement with the experimental design, the insertions were outside the inner CTD lobe (643–809 aa), which comprises the previously described (Chi G. et al., 2021) scissor helix and  $\beta$ 1– $\beta$ 5 strands required for KCC2 dimerization (Figures 1D,E).

### 3.2 Somatodendritic distribution of the KCC2-CTD mutants in neurons

Previous studies have shown that KCC2 expression and lateral diffusion in the plasma membrane strongly depend on the CTD phosphorylation (Conway et al., 2017; Friedel et al., 2015; Heubl et al., 2017; Inoue et al., 2012; Lee et al., 2007) and interaction with regulatory proteins (Chamma et al., 2013; Li et al., 2007; Llano et al., 2015). Since most 5-aa insertions were located in the CTD outer lobe, we expected their possible effect on the KCC2 somatodendritic distribution. Thus, dissociated cortical cultures were transiently



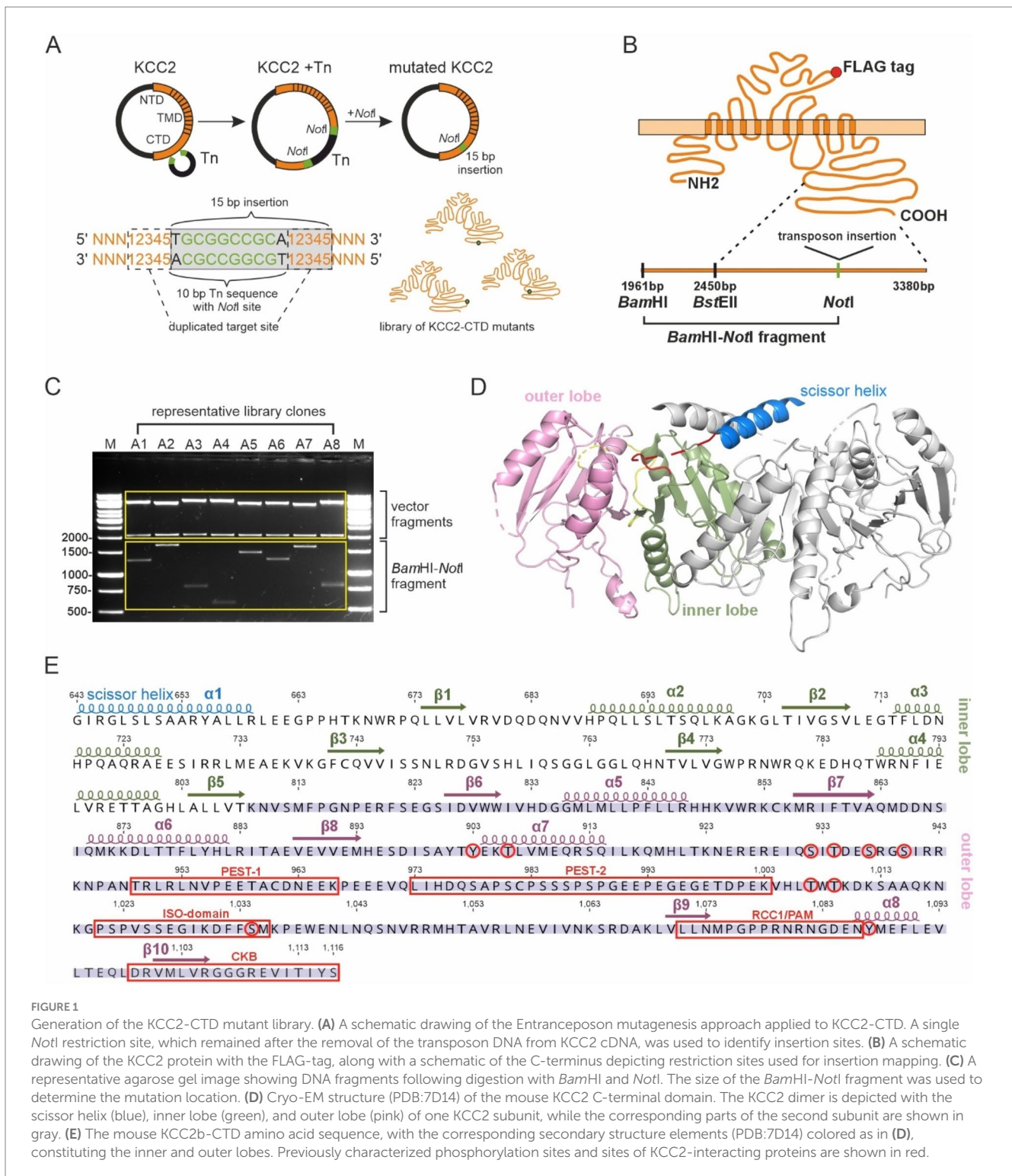


**FIGURE 1**  
Generation of the KCC2-CTD mutant library. **(A)** A schematic drawing of the Entraposepon mutagenesis approach applied to KCC2-CTD. A single *NotI* restriction site, which remained after the removal of the transposon DNA from KCC2 cDNA, was used to identify insertion sites. **(B)** A schematic drawing of the KCC2 protein with the FLAG-tag, along with a schematic of the C-terminus depicting restriction sites used for insertion mapping. **(C)** A representative agarose gel image showing DNA fragments following digestion with *Bam*HI and *Not*I. The size of the *Bam*HI-*Not*I fragment was used to determine the mutation location. **(D)** Cryo-EM structure (PDB:7D14) of the mouse KCC2 C-terminal domain. The KCC2 dimer is depicted with the scissor helix (blue), inner lobe (green), and outer lobe (pink) of one KCC2 subunit, while the corresponding parts of the second subunit are shown in gray. **(E)** The mouse KCC2b-CTD amino acid sequence, with the corresponding secondary structure elements (PDB:7D14) colored as in **(D)**, constituting the inner and outer lobes. Previously characterized phosphorylation sites and sites of KCC2-interacting proteins are shown in red.

transfected with 96 randomly selected KCC2 mutants and analyzed using antibodies recognizing the FLAG-tag placed in the 3rd extracellular loop, outside the previously characterized glycosylation sites and secondary structure elements. The transfection mixture also contained GFP, enabling the identification of the transfected neurons and the analysis of the effect of KCC2-CTD mutants on the morphology of dendritic trees in transfected neurons. For each mutant, FLAG-immunoreactivity (FLAG-ir) in the transfected

neurons was examined considering several parameters: (1) total signal intensity, (2) somatic distribution, and (3) distribution in proximal and distal dendrites.

Out of 96 analyzed mutants, 14 demonstrated ectopic FLAG-ir and/or GFP expression patterns and were sequenced to identify positions of the 5-aa insertion. Ten sequenced mutants (Table 1) with unique insertion sites located outside the previously characterized KCC2 regulatory motifs PEST-1, PEST-2, ISO-domain, CKB, RCC1/

TABLE 1 Summary for the immunocytochemical analysis of the selected KCC2-CTD mutants.

CTD-mutant	FLAG-immunoreactivity			Morphology		Notes
	Cell body	Primary dendrites	Other dendrites	Dendritic tree	Cell body	
A7	++	+/-	-	Lamellipodia	Distorted shape	Somatic expression
A8	+	+/-	-	Short distorted dendrites, lamellipodia		
B1	+/-	-	-	Distorted shape, beading	Distorted shape	
B8	+++	+++	+++	Distorted, beading, few dendrites per cell		Strong FLAG-ir in dendritic spines
C1	+++	+++	+++	Distorted, beading, few dendrites per cell		Strong FLAG-ir in dendritic spines
C10	++	+	-	Distorted dendrites, lamellipodia	Distorted shape	
C11	++	++	+	Short distorted dendrites, beading, lamellipodia	Distorted shape	
E4	+++	++	++	Short dendrites, beading, lamellipodia		
F7	++	++	+	Short dendrites, many spines/filopodia		Strong FLAG-ir in dendritic spines
F11	+++	++	+	Multiple thin dendrites		

Expression level: +/- poor, + weak, ++ moderate, +++ strong.

PAM (Supplementary Figure 1) were chosen for detailed functional characterization. The selected mutations were found within both the unstructured linker-type sequences and the highly conserved  $\alpha$ -helices and  $\beta$ -strands (Figure 2A).

Except for A8 and B1, all selected mutants demonstrated moderate to high levels of the somatic FLAG-ir (Supplementary Figure 2). Dendritic levels of FLAG-ir varied significantly, being highest for B8 and C1, but lowest for A7, A8, and C10 mutants. Somatic morphology was affected in neurons expressing A7, B1, C10, and C11 mutants, whereas dendritic morphology was distorted in nearly all mutants. Alterations included lamellipodia formation, malformed, short, or thin dendrites, as well as focal swelling of dendrites, known as dendritic blebbing.

The observed morphological changes in soma and dendrites could result from the altered intracellular ion balance due to the altered K-Cl cotransporter activity (Weilinger et al., 2022) or from the malformed cytoskeleton caused by the impaired KCC2 interaction with the previously identified actin-regulating partners, e.g., 4.1 N and  $\beta$ -PIX (Li et al., 2007; Llano et al., 2015). The position of the KCC2 mutants in the outer lobe suggests that both scenarios are possible (Figures 2B–D). One group of the mutants (A7, C1, C11, and F11) is located near the interface between the transmembrane domain (TMD) and CTD, known to contribute to the interaction with the KCC2 N-terminal inhibitory peptide that directly regulates KCC2 efflux activity (Zhang et al., 2021). Mutants from another group (A8, B1, B8, C10, and E4) are located on the external side surface of the KCC2-CTD, potentially disrupting the interaction with regulatory proteins. Therefore, in the next step, we measured the K-Cl cotransporter activity of the selected mutants.

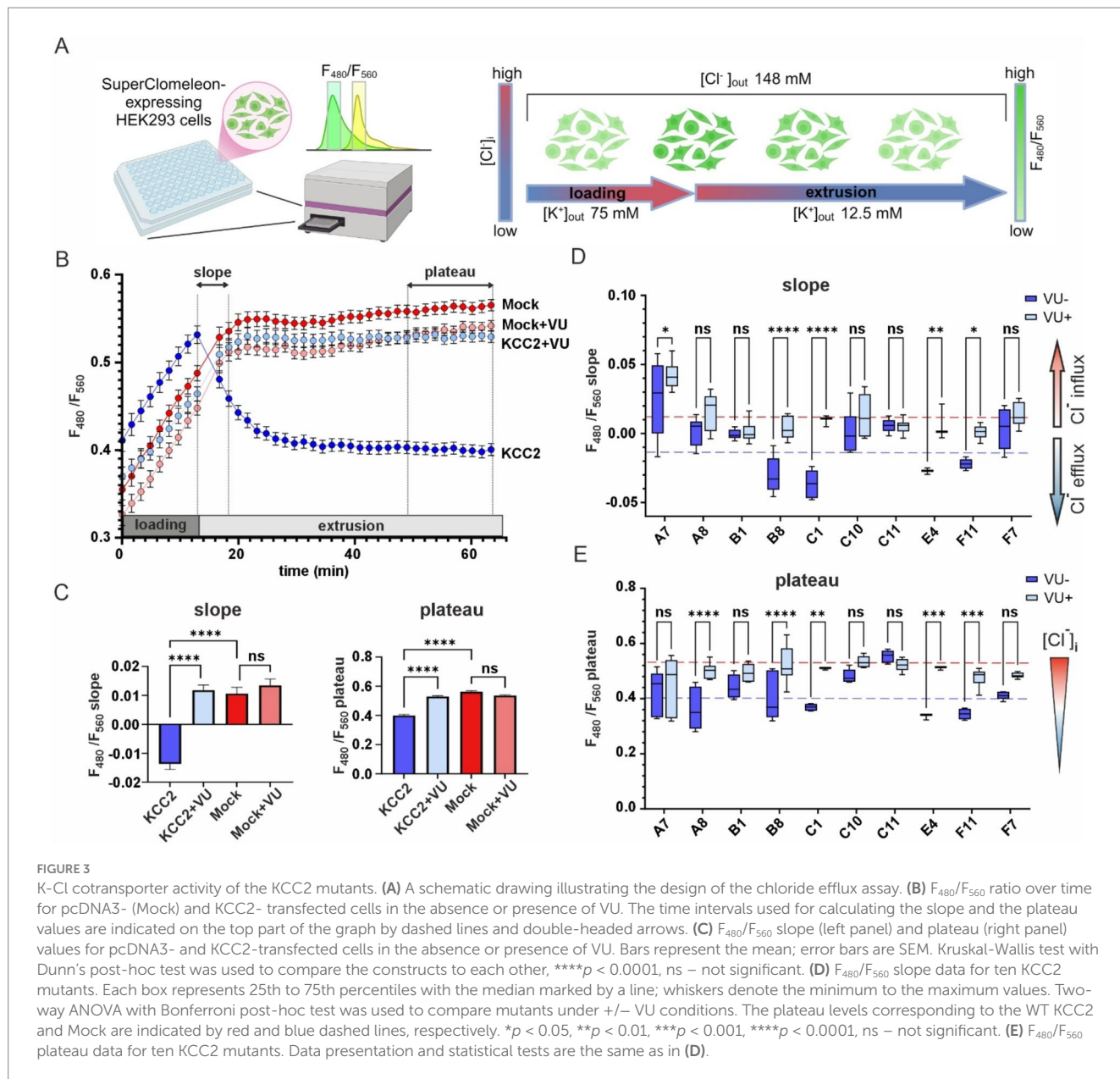
### 3.3 Cl<sup>-</sup> efflux activity of the KCC2-CTD mutants in HEK293 cells

To assess the K-Cl cotransport activity of the KCC2 mutants, we utilized the Cl<sup>-</sup> – sensitive fluorescent reporter SuperClomeleon (Grimley et al., 2013). The standard assay began by perfusing the HEK293 cells with a high-K<sup>+</sup> solution to promote an increase in intracellular [Cl<sup>-</sup>]<sub>i</sub> (loading step), followed by a low-K<sup>+</sup> solution to induce KCC2-driven Cl<sup>-</sup> efflux, thereby reducing intracellular [Cl<sup>-</sup>]<sub>i</sub> (extrusion step) (Figure 3A). The rate of [Cl<sup>-</sup>]<sub>i</sub> decline and the steady-state plateau level of [Cl<sup>-</sup>]<sub>i</sub> achieved at the end of the extrusion step were assessed by monitoring the emitted SuperClomeleon fluorescence at 480 nm ([Cl<sup>-</sup>]<sub>i</sub>-insensitive Cerulean fluorescence) and 560 nm ([Cl<sup>-</sup>]<sub>i</sub>-sensitive YFP fluorescence). The F<sub>480</sub>/F<sub>560</sub> ratio was used as an indicator of the [Cl<sup>-</sup>]<sub>i</sub>, with a lower ratio corresponding to lower [Cl<sup>-</sup>]<sub>i</sub> levels.

HEK293 cells transfected with the nonmutant KCC2 construct showed a steep increase of F<sub>480</sub>/F<sub>560</sub> ratio from 0.41 ± 0.01 to 0.53 ± 0.01 during the loading step, a robust drop to 0.46 ± 0.01 during first 5 min of the extrusion step and continued to slowly decrease until reaching a plateau level of 0.40 ± 0.06 during the last 10 min of the extrusion step (Figure 3B, dark blue). KCC2-specific inhibitor VU0463271 (VU) completely abolished the F<sub>480</sub>/F<sub>560</sub> ratio decrease during the extrusion step (Figure 3B, light blue). HEK293 cells lacking KCC2 (mock-transfected), with or without VU (Figure 3B, dark and light red curves, respectively), did not reveal any drop in F<sub>480</sub>/F<sub>560</sub> ratio. These data indicate that the slope of the F<sub>480</sub>/F<sub>560</sub> curve during the first 5 min and the F<sub>480</sub>/F<sub>560</sub> ratio averaged during the last 10 min of the extrusion step can both







extrusion solution has low  $[K^+]$  and the driving force for  $K^+$  is directed outward,  $Cl^-$  influx under these conditions implies that A7 mutant has lost either the coupling between  $K^+$  and  $Cl^-$  ions or the ion selectivity. The remaining mutants (B8, C1, E4, and F11) exhibited significant differences between +/- VU conditions for both the slope and the plateau measurements, indicating that these mutants possess  $Cl^-$ -extruding activity. Notably, all four mutations are located in poorly conserved CTD regions (Figure 2) outside known secondary structural motifs (see Table 2). Also, three out of four mutants (B8, C1, and F11) are located outside previously characterized KCC2-regulatory sites, while one (E4) is next to the previously characterized S940 phosphorylation site (Supplementary Figure 1). Interestingly, B8 and C1 demonstrated prominent negative slopes, indicating faster  $Cl^-$  extrusion kinetics compared to WT KCC2 (blue dashed line in Figure 3D). To sum up, mutating the distal KCC2-CTD region modulates the K-Cl cotransporter function both negatively and, what is important, positively.

### 3.4 KCC2-CTD mutants reveal different glycosylation patterns in the HEK293 cells

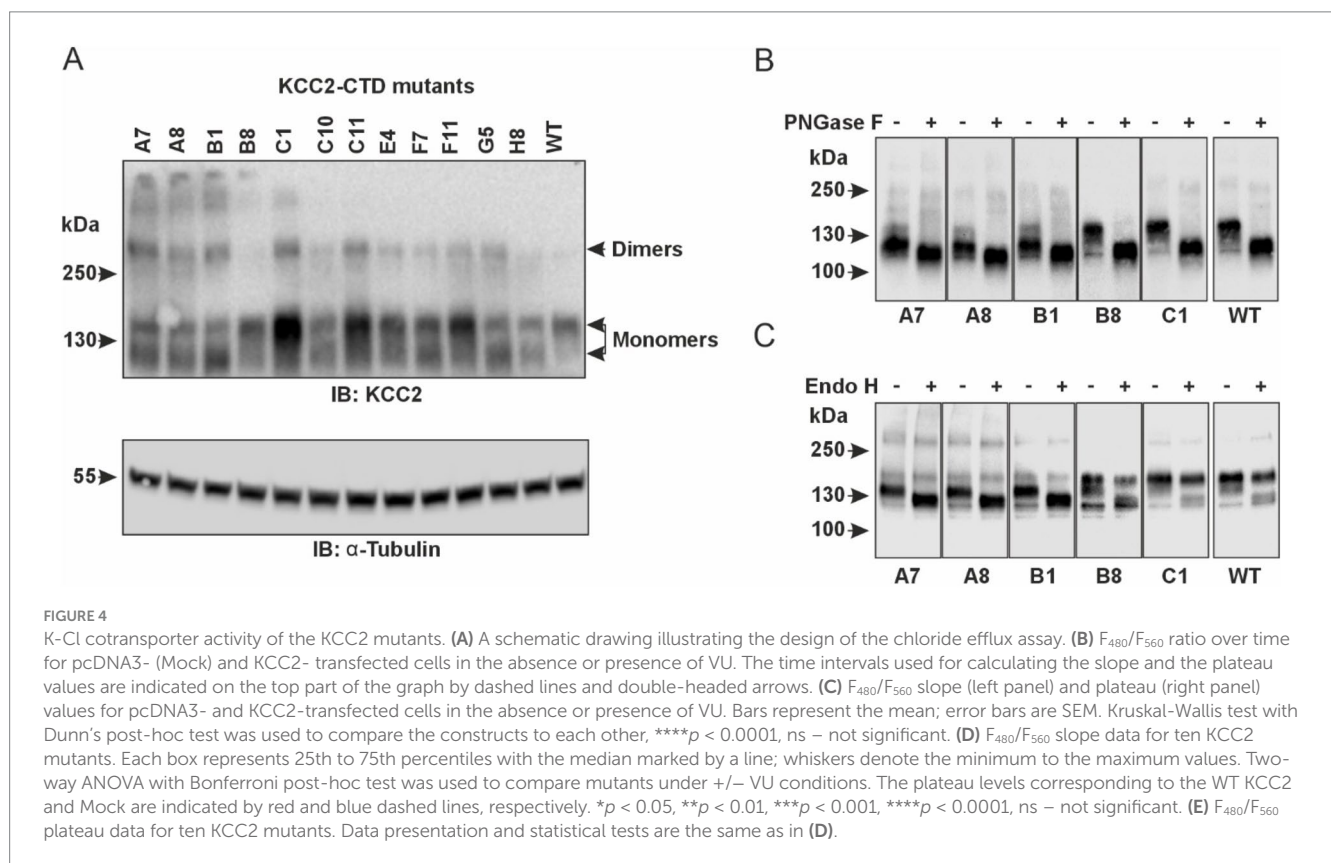
The observed effect of the KCC2-CTD mutations on K-Cl cotransporter function may result from changes in  $Cl^-$  extrusion kinetics or alterations in KCC2 abundance in the plasma membrane. Since protein trafficking to the plasma membrane is intimately linked to its glycosylation status, we next analyzed the glycosylation pattern of KCC2 mutants. Two protein bands with molecular weights close to the predicted non-glycosylated KCC2b polypeptide (123.6-kDa) have been previously reported in KCC2-overexpressing HEK293 lysates by SDS-PAGE (Agez et al., 2017; Blaesse et al., 2006; Williams et al., 1999), implying at least two glycosylation states (Payne et al., 1996; Kok et al., 2024).

In agreement with the previous studies, our western blot data revealed two monomeric KCC2 bands close to ~130-kDa in total protein lysates of HEK293 cells expressing CTD mutants (Figure 4A).



**TABLE 2** VU-sensitive Cl<sup>-</sup> extrusion activities of the KCC2 mutants, along with positions of mutations, insertion sequences, and structural elements at the mutation positions according to PDB: 7D14.

Mutant	Position (aa)	Insert	Structural element	VU-sensitive Cl <sup>-</sup> flux (KCC2 = 100%)	
				Slope	Plateau
F11	816	VRPHP		90 ± 7	102 ± 5
C1	817	CGRTG		232 ± 7	104 ± 6
F7	830	LRPQW	β6-strand	32 ± 27	64 ± 4
C11	846	CGRIL	α5-helix	-15 ± 9	-4 ± 6
A7	853	CGRRR		60 ± 39	35 ± 16
B8	865	RPQQM		137 ± 20	96 ± 17
C10	890	CGRME	β8-strand	39 ± 30	50 ± 7
E4	936	CGRTD		68 ± 31	65 ± 29
B1	1,066	CGRTR	3-aa upstream β9	-4 ± 5	50 ± 9
A8	1,069	CGRTK	β9-strand	56 ± 15	105 ± 15
Mock				0 ± 10	0 ± 4



The upper one (~140-kDa), presumably corresponding to the fully glycosylated KCC2 form, was prevalent in the cells expressing the WT KCC2 as well as B8, C1, C11, E4, and F11 CTD mutants. The remaining mutants (A7, A8, B1, C10, F7) showed comparable intensity for the upper (~140-kDa) and the lower (~125-kDa) KCC2 bands. To test whether N-glycosylation causes the observed difference in molecular weights of the two KCC2 monomeric bands, HEK293 lysates were treated with peptide-N-glycosidase F (PNGase F), known to remove most of the N-linked oligosaccharides (Tarentino and Plummer, 1994). Indeed, PNGase F treatment shifted both the 140-kDa and the 125-kDa bands for WT KCC2 and all CTD mutants down to the predicted

123.6-kDa molecular weight for the non-glycosylated KCC2 (Figure 4B). To examine whether the upper 140-kDa band corresponds to the mature Golgi-type glycosylation pattern rather than to the immature ER-type, HEK293 protein lysates were treated with the Endoglycosidase H (Endo H). Endo H cleaves oligosaccharides added to the proteins in the ER but not those processed in the Golgi, and thus is often used for assessing the extent of protein trafficking from ER toward the plasma membrane. As expected, the upper 140-kDa band, but not the lower 125-kDa, was resistant to the Endo H treatment (Figure 4C), thus pointing at its mature N-glycosylation pattern acquired in the Golgi by the B8, C1, C11, E4, and F11 CTD mutants.

Based on glycosylation and Cl<sup>-</sup> efflux data, the analyzed KCC2-CTD mutants could be divided into two groups. The first group includes the B8, C1, E4, and F11 mutants, which exhibited both high Cl<sup>-</sup> efflux activity and a predominant Golgi glycosylation pattern (140-kDa band). The second group comprises the A7, A8, B1, C10, and F7 mutants, which showed no VU-sensitive Cl<sup>-</sup> efflux activity and displayed an immature ER-like glycosylation pattern – indicative of low plasma membrane expression. The immature glycosylation pattern in this group could be attributed to impaired KCC2 conformation, leading to a failure to exit the ER, which in turn prevents KCC2 trafficking to the Golgi and the plasma membrane. In most cases, retention of KCC2 mutants in the ER may explain the low Cl<sup>-</sup> efflux activity. Interestingly, the C11 mutant lacked VU-sensitive Cl<sup>-</sup> efflux activity but exhibited a highly mature glycosylation pattern, suggesting that the main effect of the mutation was impairment of the transporter’s kinetic activity rather than its trafficking to the plasma membrane.

### 3.5 The abundance of the KCC2-CTD mutants in the neuronal plasma membrane correlates with their glycosylation patterns in HEK293 cells

To test whether the glycosylation patterns observed in HEK293 cells correlate with the abundance of the KCC2-CTD mutants in the neuronal plasma membrane, we analyzed their membrane expression

in dissociated cortical cultures. We selected mutants representing all three glycosylation groups: A7 and A8 (immature glycosylation and no Cl<sup>-</sup> extrusion activity), B8 and C1 (mature glycosylation and high Cl<sup>-</sup> extrusion activity), and C11 (intermediate glycosylation and no Cl<sup>-</sup> extrusion activity). To visualize KCC2 expression at the neuronal plasma membrane, cortical cultures were transfected with the corresponding KCC2 expression constructs, and FLAG-ir was assessed using live-cell surface immunolabeling protocol (Chamma et al., 2013; Friedel et al., 2017). This protocol consists of two steps (Figure 5A): first, revealing FLAG-tags of the KCC2 molecules present in the plasma membrane of non-permeabilized living cells (“Extracellular” in Figure 5B); and second, detecting FLAG-tags in KCC2 molecules in both the plasma membrane and intracellular compartments of permeabilized PFA-fixed cells “Total” in Figure 5B). The ratio of the two signals serves as a measure of the KCC2 plasmalemmal abundance.

Consistent with their low Cl<sup>-</sup> efflux and immature glycosylation pattern, the A7 and A8 mutants exhibited much lower membrane abundance compared to WT KCC2 (Figure 5C, A7: 0.03 ± 0.01, *p* = 0.004; A8: 0.16 ± 0.04, *p* = 0.004, one-sample Wilcoxon test). In contrast, B8 mutant was presented in the plasma membrane at a level three times higher than WT KCC2 (Figure 5C, B8: 2.96 ± 1.16, *p* = 0.027, one-sample Wilcoxon test) correlating with its high Cl<sup>-</sup> efflux and mature glycosylation pattern. C1 and C11 mutants showed no difference in either the membrane abundance (Figure 5C) or glycosylation patterns (Figure 4) compared to WT KCC2. Given that C1 exhibited high Cl<sup>-</sup> efflux while C11 showed no detectable Cl<sup>-</sup> extrusion activity, these data suggest that the mechanisms regulating

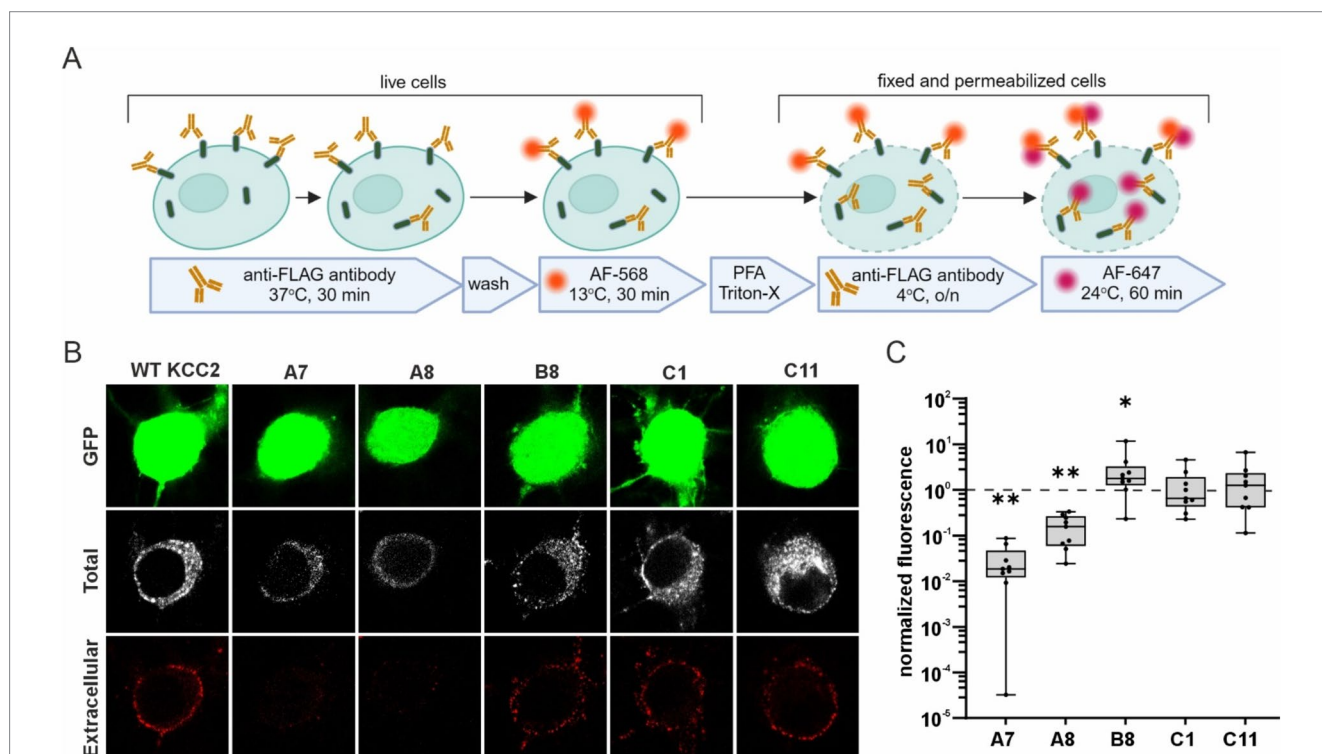


**FIGURE 5** Surface expression of the KCC2-CTD mutants in cortical neurons. **(A)** A schematic drawing illustrating the live-cell labeling protocol. **(B)** Representative images of cortical neurons expressing WT KCC2 and selected KCC2-CTD mutants. Panels show GFP expression, total FLAG-ir (“Total”), and extracellular FLAG-ir (“Extracellular”). **(C)** Surface expression of the KCC2-CTD mutants normalized to that of WT KCC2 (indicated by the dashed line on the plot). Each box represents 25th to 75th percentiles with the median marked by a line; whiskers denote the minimum to the maximum values; one sample Wilcoxon test, \**p* < 0.05, \*\**p* < 0.01.

C11 trafficking to the plasma membrane and K-Cl cotransporter activity may function independently.

### 3.6 Somatodendritic chloride gradient measured in the cultured cortical neurons

KCC2-mediated neuronal Cl<sup>-</sup> efflux is known to be sufficient for maintaining the somatodendritic E<sub>GABA</sub> gradient (ΔE<sub>GABA</sub>) under whole-cell clamp conditions with a constant somatic Cl<sup>-</sup> load (Jarolimek et al., 1999; Khirug et al., 2005). To assess the transport activity of KCC2-CTD mutants with the mature (B8, C1) and intermediate (F11) glycosylation patterns, we measured their ΔE<sub>GABA</sub> in immature DIV 3 dissociated cortical cultures, when the impact of the endogenous KCC2 is negligible (Khirug et al., 2005) (Figure 6).

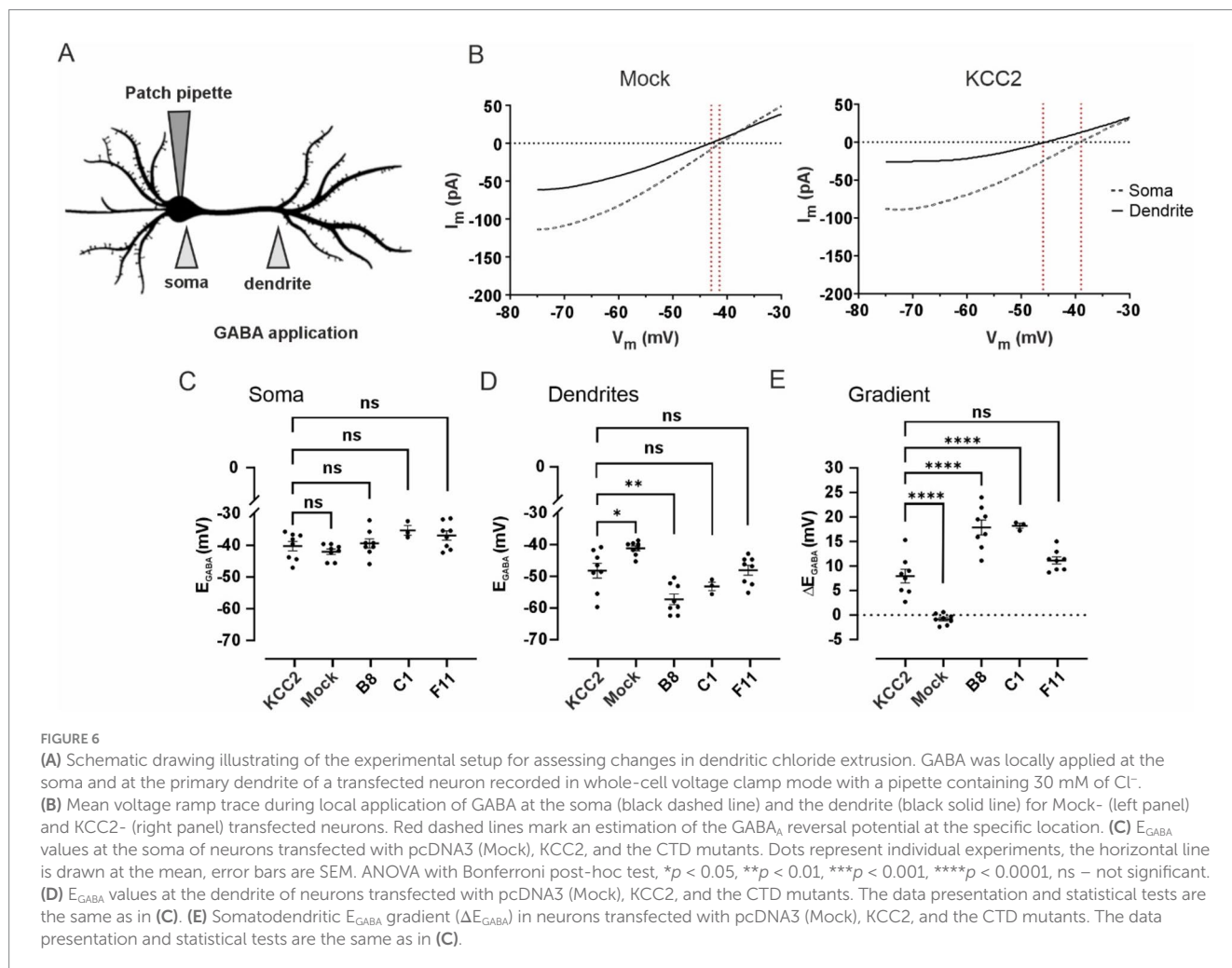
Mock-transfected neurons revealed no significant ΔE<sub>GABA</sub>: -0.8 ± 0.4 mV, with somatic E<sub>GABA</sub> -42.0 ± 0.9 mV and dendritic E<sub>GABA</sub> -41.2 ± 0.8 mV (Figures 6B–E). Transient transfection (24 h) of WT KCC2 resulted in a robust ΔE<sub>GABA</sub> of 8.0 ± 1.4 mV, with somatic and dendritic E<sub>GABA</sub> values of -40.3 ± 1.5 mV and -48.2 ± 2.3 mV, respectively. Neurons transfected with the F11 mutant (intermediate glycosylation pattern) exhibited ΔE<sub>GABA</sub> = 11.1 ± 0.7 mV (somatic E<sub>GABA</sub> - 36.9 ± 1.5 mV and dendritic E<sub>GABA</sub> -48.1 ± 1.6 mV), though the difference from WT KCC2 ΔE<sub>GABA</sub> was not statistically significant.

A much steeper ΔE<sub>GABA</sub> = 17.9 ± 1.5 mV was detected in neurons transfected with the B8 mutant (mature glycosylation pattern) with the somatic and dendritic E<sub>GABA</sub> -39.4 ± 1.5 mV and -57.2 ± 1.7 mV, respectively. Similarly to B8, neurons transfected with C1 mutant exhibited ΔE<sub>GABA</sub> of 17.9 ± 0.5 mV, with somatic and dendritic E<sub>GABA</sub> of -35.8 ± 1.5 mV and -53.7 ± 1.4 mV, respectively.

This experiment corroborates the glycosylation and membrane expression data for the B8 and C1 mutants. Specifically, the significantly increased surface expression of B8 compared to WT KCC2 (Figure 5C) corresponds to the enhanced somatodendritic ΔE<sub>GABA</sub> gradient (Figure 6E). The fact that WT KCC2 and the C1 mutant exhibit similar membrane expression levels but different Cl<sup>-</sup> extrusion capacities suggests that the C1 mutation induces a CTD conformation that promotes enhanced kinetics of Cl<sup>-</sup> extrusion.

## 4 Discussion

Reduction of KCC2 activity and consequent increase in [Cl<sup>-</sup>]<sub>i</sub> are implicated in numerous neurological conditions, which makes KCC2 a potential drug target (McMoneagle et al., 2024; Tang, 2020). Enhancing Cl<sup>-</sup> extrusion by activating KCC2 has demonstrated promising outcomes in preclinical trials using mouse models of epilepsy (Jarvis et al., 2023). However, effective drug design requires





understanding of the mechanisms governing KCC2 activity. Here we report generation of a library of KCC2 mutants with single 5-aa insertions in the distal regulatory region of KCC2-CTD. Our findings reveal novel mutations that lead to accelerated KCC2-mediated Cl<sup>-</sup> extrusion under Cl<sup>-</sup> loading conditions as well as mutations that render KCC2 inactive.

We performed the initial screening of the mutants by analyzing their expression pattern in cultured neurons. The functional presentation of KCC2 on the neuronal membrane is essential for its activity, thus we expected that an aberrant expression of a mutant might correlate with its altered activity. Indeed, out of ten mutants with the aberrant expression that were selected based on immunocytochemical analysis, five (A7, B1, C10, C11, and F7) did not show any detectable VU-sensitive activity in the fluorescent Cl<sup>-</sup> efflux assay, one (A8) had strongly diminished activity, two (B8 and C1) had strongly enhanced activity, and only two (E4 and F11) had activity similar to WT KCC2 (Figures 3D,E).

KCC2 exists as a dimer in domain-swapping conformation (Chi X. et al., 2021; Xie et al., 2020). By design, mutagenesis in our study was restricted to the outer CTD lobe (Figures 1D, 2B–D), avoiding the previously described scissor helix and  $\beta$ 1– $\beta$ 5 strands required for KCC2 dimerization (Chi G. et al., 2021; Zhang et al., 2021), thus we do not expect that these mutations directly interfere with dimerization. The maturation process of KCC2 protein includes glycosylation at specific sites within the third extracellular loop (Agez et al., 2017). KCC2 expression in the plasma membrane is known to correlate with the transporter glycosylation pattern (Hartmann and Nothwang, 2015). Although the mutations reported in this study were limited to the KCC2-CTD and could not directly alter KCC2 glycosylation sites, faulty processing of KCC2 mutants or their inability to form dimers may lead to retention in the endoplasmic reticulum ER (Trombetta and Parodi, 2003), resulting in an immature glycosylation pattern (Kok et al., 2024). Alterations in protein conformation, disruption of ER exit signals, and interference with ER chaperones and regulatory proteins are all known to affect protein exit from the ER and, consequently, its abundance in the plasma membrane (Anelli and Panina-Bordignon, 2019). For example, mutating the C-terminal di-acidic motif has been shown to prevent NKCC2 from exiting the ER and reaching the plasma membrane, causing it to accumulate in the ER (Bakhos-Douaihy et al., 2022).

The regulation of KCC2 surface expression involves multiple regulatory sites within the KCC2-CTD, including di-leucine motif (Zhao et al., 2008), S940 phosphorylation site (Lee et al., 2007), and a hydrophobic tetrapeptide sequence (VMLV) (Tang, 2016). Interestingly, none of the mutants exhibiting an immature glycosylation pattern (A7, A8, B1, and C10) had insertions proximal to these sites. However, all these insertions, except A7, were located within structural elements such as  $\alpha$ -helices or  $\beta$ -strands described recently (Zhang et al., 2021). This suggests that the poor membrane expression of these mutants is likely due to their ER retention caused by protein folding failures.

Loss-of function mutations in KCC2-CTD can result in either a reduced amount of the cotransporter in the plasma membrane or in impaired chloride extrusion without altering its membrane expression. For example, there are indications that phosphorylation status at T906/T1007 might directly modulate intrinsic transport activity of KCC2 (Moore et al., 2018). Similarly, E50\_Q93del and M415V mutations associated with epilepsy of infancy with migrating focal

seizures suppress Cl<sup>-</sup> extrusion without affecting KCC2 cell surface expression (Saitou et al., 2016). Previous studies have also shown that even single-amino acid substitutions (L675A and R1049C) could strongly affect the KCC2 kinetic activity without substantial changes in their plasma membrane expression (Döding et al., 2012; Kahle et al., 2014).

Our western blot data showed that, in most cases, the glycosylation pattern of the CTD mutants corresponded to their Cl<sup>-</sup> extrusion activity. For example, inactive mutants A7, B1, and C10 did not display the fully glycosylated form on the western blot, while mutants with high Cl<sup>-</sup> extrusion activity, such as B8 and C1, exhibited a prominent glycosylated band (Figures 3D,E 4B). Interestingly, the C11 mutant displayed a mature glycosylation pattern but did not demonstrate any detectable VU-sensitive Cl<sup>-</sup> efflux in the Cl<sup>-</sup> extrusion assay. The live-cell labeling assay conducted in neurons confirmed that both C11 and C1 mutants exhibited membrane abundance similar to WT KCC2 (Figure 5B). One possible explanation for the inactivity of the C11 mutant could be that KCC2 distribution in the plasma membrane might also influence its functional state. Two previous studies highlighted a special role of lipid rafts in regulating KCC2 activity (Watanabe et al., 2009; Hartmann et al., 2009). Another possibility is that KCC2 activity can be controlled independently of its membrane expression.

While numerous loss-of-function KCC2 mutations have been described previously both in humans and rodents (McMoneagle et al., 2024), gain-of-function mutations are far less common. To the best of our knowledge, two hyperactive KCC2 mutants have been described so far, both affecting KCC2 phosphorylation status. The first is the double mutant T906A/T1007A that renders impossible the phosphorylation of KCC2 at these sites (Rinehart et al., 2009). Cultured neurons ectopically expressing the T906A/T1007A mutant exhibited strongly hyperpolarized E<sub>GABA</sub> values compared to WT neurons (Inoue et al., 2012; Moore et al., 2019). The second is a phosphomimetic S937D, which showed an increased KCC2 activity in HEK293 cells and in neurons from transgenic T934A/S937D mice (Radulovic et al., 2023; Weber et al., 2014). In the current study, we present two more mutants with enhanced Cl<sup>-</sup> extrusion capacity, B8 and C1. Both mutants have insertions located outside known structural and phosphorylation motifs (Table 2 and Supplementary Figure 1) in regions surrounding highly conserved  $\beta$ 6– $\alpha$ 5– $\beta$ 7 structural elements (Figure 2A). B8 insertion site is moderately conserved among KCC2 paralogs, indicating that B8 mutation might disrupt an unidentified regulatory element. In contrast, C1 site shows low homology with other KCCs, and it appears that the specific 5-amino acid insertion in C1 (CGRTG at residue 817) renders the mutated KCC2 hyperactive. Supporting this, the F11 mutant, which contains a VRPHP insertion at residue 816, just one amino acid upstream of C1, exhibits normal Cl<sup>-</sup> extrusion kinetics.

In conclusion, we utilized the Mu transposon-based mutagenesis system to generate a mutant library targeting KCC2-CTD, which contained 221 mutants within ~300 aa distal CTD region and 67 mutants in the proximal 3'UTR. We analyzed mutants with ectopic neuronal expression to explore how specific mutations affect Cl<sup>-</sup> extrusion activity and membrane expression. We identified both gain-of-function and loss-of-function mutations and confirmed that the high cotransporter activity overall correlated with the mature glycosylation status. Nevertheless, one loss-of-function mutant (C11)

demonstrated a mature glycosylation pattern and no cotransporter activity suggesting that the KCC2 kinetic activity can be regulated in parallel to a membrane expression.

Given the diverse regulatory functions of KCC2-CTD, our CTD insertion library promotes identification of novel motifs modulating various aspects of KCC2 activity. Further systematic analysis of the positions of the CTD mutations could provide valuable insights into the mechanisms governing KCC2 regulation and potentially discover new targets for therapeutic intervention in neurological disorders.

## Data availability statement

The raw data supporting the conclusions of this article will be made available by the authors, without undue reservation.

## Ethics statement

The animal study was approved by the Etelä-Suomen aluehallintovirasto. The study was conducted in accordance with the local legislation and institutional requirements.

## Author contributions

PU: Conceptualization, Data curation, Formal analysis, Investigation, Methodology, Project administration, Resources, Supervision, Validation, Visualization, Writing – original draft, Writing – review & editing. SF: Formal analysis, Investigation, Writing – review & editing. CK: Investigation, Writing – review & editing, Formal analysis, Visualization. AG: Investigation, Writing – review & editing, Resources. FR: Investigation, Writing – review & editing. TS: Investigation, Writing – review & editing. SS: Investigation, Writing – review & editing. CDS: Data curation, Formal analysis, Funding acquisition, Investigation, Supervision, Visualization, Writing – review & editing. TK: Visualization, Writing – review & editing, Funding acquisition, Supervision, Validation. CR: Conceptualization, Funding acquisition, Project administration, Supervision, Writing – review & editing. AL: Conceptualization, Data curation, Formal analysis, Funding acquisition, Investigation, Methodology, Project administration, Resources, Software, Supervision, Validation, Visualization, Writing – original draft, Writing – review & editing.

## Funding

The author(s) declare financial support was received for the research, authorship, and/or publication of this article. HiLIFE proof

## References

- Acton, B. A., Mahadevan, V., Mercado, A., Uvarov, P., Ding, Y., Pressey, J., et al. (2012). Hyperpolarizing GABAergic transmission requires the KCC2 C-terminal ISO domain. *J. Neurosci. Off. J. Soc. Neurosci.* 32, 8746–8751. doi: 10.1523/JNEUROSCI.6089-11.2012
- Agez, M., Schultz, P., Medina, I., Baker, D. J., Burnham, M. P., Cardarelli, R. A., et al. (2017). Molecular architecture of potassium chloride co-transporter KCC2. *Sci. Rep.* 7:16452. doi: 10.1038/s41598-017-15739-1
- Anelli, T., and Panina-Bordignon, P. (2019). How to avoid a no-deal ER exit. *Cells* 8, 1–16. doi: 10.3390/CELLS8091051
- Bakhos-Douaihy, D., Seaayfan, E., Frachon, N., Demaretz, S., Kömhoff, M., and Laghmani, K. (2022). Diacidic motifs in the carboxyl terminus are required for ER exit and translocation to the plasma membrane of NKCC2. *Int. J. Mol. Sci.* 23, 1–18. doi: 10.3390/IJMS232112761

of concept grant 2023, AoF 332354 to AL; AoF 341361 to CR. Jane and Aatos Erkkö foundation grant to TK; AoF 333096 and 335956 to CDS, Center for International Mobility CIMO to TS.

## Acknowledgments

We are grateful to Harri Savilahti (University of Turku, Finland) for his valuable insights and guidance on library generation. We would like to thank Seija Lågas for excellent assistance in neuronal culturing. Figures 1A, 5A were created in BioRender.

## Conflict of interest

The authors declare that the research was conducted in the absence of any commercial or financial relationships that could be construed as a potential conflict of interest.

The author(s) declared that they were an editorial board member of *Frontiers*, at the time of submission. This had no impact on the peer review process and the final decision.

## Generative AI statement

The author(s) declare that Generative AI was used in the creation of this manuscript.

## Publisher's note

All claims expressed in this article are solely those of the authors and do not necessarily represent those of their affiliated organizations, or those of the publisher, the editors and the reviewers. Any product that may be evaluated in this article, or claim that may be made by its manufacturer, is not guaranteed or endorsed by the publisher.

## Supplementary material

The Supplementary material for this article can be found online at: <https://www.frontiersin.org/articles/10.3389/fnmol.2024.1505722/full#supplementary-material>

- Barmashenko, G., Hefft, S., Aertens, A., Kirschstein, T., and Köhling, R. (2011). Positive shifts of the GABAA receptor reversal potential due to altered chloride homeostasis is widespread after status epilepticus. *Epilepsia* 52, 1570–1578. doi: 10.1111/j.1528-1167.2011.03247.x
- Blaesse, P., Guillemain, I., Schindler, J., Schweizer, M., Delpire, E., Khiroug, L., et al. (2006). Oligomerization of KCC2 correlates with development of inhibitory neurotransmission. *J. Neurosci.* 26, 10407–10419. doi: 10.1523/JNEUROSCI.3257-06.2006
- Boulenguez, P., Liabeuf, S., Bos, R., Bras, H., Jean-Xavier, C., Brocard, C., et al. (2010). Down-regulation of the potassium-chloride cotransporter KCC2 contributes to spasticity after spinal cord injury. *Nat. Med.* 16, 302–307. doi: 10.1038/nm.2107
- Chamma, I., Heubl, M., Chevy, Q., Renner, M., Moutkine, I., Eugène, E., et al. (2013). Activity-dependent regulation of the K<sup>+</sup>/Cl<sup>-</sup> transporter KCC2 membrane diffusion, clustering, and function in hippocampal neurons. *J. Neurosci.* 33, 15488–15503. doi: 10.1523/JNEUROSCI.5889-12.2013
- Chi, G., Ebenhoch, R., Man, H., Tang, H., Tremblay, L. E., Reggiano, G., et al. (2021). Phospho-regulation, nucleotide binding and ion access control in potassium-chloride cotransporters. *EMBO J.* 40:e107294. doi: 10.15252/emboj.2020107294
- Chi, X., Li, X., Chen, Y., Zhang, Y., Su, Q., and Zhou, Q. (2021). Cryo-EM structures of the full-length human KCC2 and KCC3 cation-chloride cotransporters. *Cell Res.* 31, 482–484. doi: 10.1038/s41422-020-00437-x
- Conti, L., Palma, E., Rosetti, C., Lauro, C., Cipriani, R., de Groot, M., et al. (2011). Anomalous levels of Cl<sup>-</sup> transporters cause a decrease of GABAergic inhibition in human peritumoral epileptic cortex. *Epilepsia* 52, 1635–1644. doi: 10.1111/j.1528-1167.2011.03111.x
- Conway, L. C., Cardarelli, R. A., Moore, Y. E., Jones, K., McWilliams, L. J., Baker, D. J., et al. (2017). N-Ethylmaleimide increases KCC2 cotransporter activity by modulating transporter phosphorylation. *J. Biol. Chem.* 292, 21253–21263. doi: 10.1074/jbc.M117.817841
- Cordshagen, A., Busch, W., Winkhofer, M., Nothwang, H. G., and Hartmann, A. M. (2018). Phosphoregulation of the intracellular termini of K-Cl cotransporter 2 (KCC2) enables flexible control of its activity. *J. Biol. Chem.* 293, 16984–16993. doi: 10.1074/jbc.RA118.004349
- Deeb, T. Z., Nakamura, Y., Frost, G. D., Davies, P. A., and Moss, S. J. (2013). Disrupted Cl<sup>-</sup> homeostasis contributes to reductions in the inhibitory efficacy of diazepam during hyperexcited states. *Eur. J. Neurosci.* 38, 2453–2467. doi: 10.1111/ejn.12241
- Döding, A., Hartmann, A. M., Beyer, T., and Nothwang, H. G. (2012). KCC2 transport activity requires the highly conserved L<sub>675</sub> in the C-terminal  $\beta$ 1 strand. *Biochem. Biophys. Res. Commun.* 420, 492–497. doi: 10.1016/j.bbrc.2012.02.147
- Friedel, P., Bregestovski, P., and Medina, I. (2013). Improved method for efficient imaging of intracellular Cl<sup>-</sup> with Cl<sup>-</sup>-sensor using conventional fluorescence setup. *Front. Mol. Neurosci.* 6:7. doi: 10.3389/fnmol.2013.00007
- Friedel, P., Kahle, K. T., Zhang, J., Hertz, N., Pisella, L. I., Buhler, E., et al. (2015). WNK1-regulated inhibitory phosphorylation of the KCC2 cotransporter maintains the depolarizing action of GABA in immature neurons. *Sci. Signal.* 8, 23–26. doi: 10.1126/scisignal.aaa0354
- Friedel, P., Ludwig, A., Pellegrino, C., Agez, M., Jawhari, A., Rivera, C., et al. (2017). A novel view on the role of intracellular tails in surface delivery of the potassium-chloride cotransporter KCC2. *ENEURO* 4:ENEURO.0055-17.2017. doi: 10.1523/ENEURO.0055-17.2017
- Grimley, J. S., Li, L., Wang, W., Wen, L., Beese, L. S., Hellinga, H. W., et al. (2013). Visualization of synaptic inhibition with an optogenetic sensor developed by cell-free protein engineering automation. *J. Neurosci. Off. J. Soc. Neurosci.* 33, 16297–16309. doi: 10.1523/JNEUROSCI.4616-11.2013
- Hartmann, A. M., Blaesse, P., Kranz, T., Wenz, M., Schindler, J., Kaila, K., et al. (2009). Opposite effect of membrane raft perturbation on transport activity of KCC2 and NKCC1. *J. Neurochem.* 111, 321–331. doi: 10.1111/j.1471-4159.2009.06343.x
- Hartmann, A. M., and Nothwang, H. G. (2015). Molecular and evolutionary insights into the structural organization of cation chloride cotransporters. *Front. Cell. Neurosci.* 8:470. doi: 10.3389/fncel.2014.00470
- Heubl, M., Zhang, J., Pressey, J. C., Al Awabdh, S., Renner, M., Gomez-Castro, F., et al. (2017). GABAA receptor dependent synaptic inhibition rapidly tunes KCC2 activity via the Cl<sup>-</sup>-sensitive WNK1 kinase. *Nat. Commun.* 8:1776. doi: 10.1038/s41467-017-01749-0
- Hübner, C. A., Stein, V., Hermans-Borgmeyer, I., Meyer, T., Ballanyi, K., and Jentsch, T. J. (2001). Disruption of KCC2 reveals an essential role of K-Cl cotransport already in early synaptic inhibition. *Neuron* 30, 515–524. doi: 10.1016/S0896-6273(01)00297-5
- Inoue, K., Furukawa, T., Kumada, T., Yamada, J., Wang, T., Inoue, R., et al. (2012). Taurine inhibits K<sup>+</sup>-Cl<sup>-</sup> cotransporter KCC2 to regulate embryonic Cl<sup>-</sup> homeostasis via with-no-lysine (WNK) protein kinase signaling pathway. *J. Biol. Chem.* 287, 20839–20850. doi: 10.1074/jbc.M111.319418
- Jarolimek, W., Lewen, A., and Misgeld, U. (1999). A furosemide-sensitive K<sup>+</sup>-Cl<sup>-</sup> cotransporter counteracts intracellular Cl<sup>-</sup> accumulation and depletion in cultured rat midbrain neurons. *J. Neurosci.* 19, 4695–4704. doi: 10.1523/JNEUROSCI.19-12-04695.1999
- Järvelä, V., Hamze, M., Komulainen-Ebrahim, J., Rahikkala, E., Piispala, J., Kallio, M., et al. (2024). A novel pathogenic SLC12A5 missense variant in epilepsy of infancy with migrating focal seizures causes impaired KCC2 chloride extrusion. *Front. Mol. Neurosci.* 17:1372662. doi: 10.3389/fnmol.2024.1372662
- Jarvis, R., Josephine Ng, S. F., Nathanson, A. J., Cardarelli, R. A., Abiraman, K., Wade, F., et al. (2023). Direct activation of KCC2 arrests benzodiazepine refractory status epilepticus and limits the subsequent neuronal injury in mice. *Cell Rep. Med.* 4:100957. doi: 10.1016/j.xcrm.2023.100957
- Kahle, K. T., Merner, N. D., Friedel, P., Silayeva, L., Liang, B., Khanna, A., et al. (2014). Genetically encoded impairment of neuronal KCC2 cotransporter function in human idiopathic generalized epilepsy. *EMBO Rep.* 15, 766–774. doi: 10.15252/embr.201438840
- Khirug, S., Huttu, K., Ludwig, A., Smirnov, S., Voipio, J., Rivera, C., et al. (2005). Distinct properties of functional KCC2 expression in immature mouse hippocampal neurons in culture and in acute slices. *Eur. J. Neurosci.* 21, 899–904. doi: 10.1111/j.1460-9568.2005.03886.x
- Kok, M., Hartnett-Scott, K., Happe, C. L., Mac Donald, M. L., Aizenman, E., and Brodsky, J. L. (2024). The expression system influences stability, maturation efficiency, and oligomeric properties of the potassium-chloride co-transporter KCC2. *Neurochem. Int.* 174:105695. doi: 10.1016/j.neuint.2024.105695
- Lee, H., Walker, J., Williams, J., Goodier, R., Payne, J., and Moss, S. (2007). Direct protein kinase C-dependent phosphorylation regulates the cell surface stability and activity of the potassium chloride cotransporter KCC2. *J. Biol. Chem.* 282, 29777–29784. doi: 10.1074/jbc.M705053200
- Lee, K. L., Abiraman, K., Lucaj, C., Ollerhead, T. A., Brandon, N. J., Deeb, T. Z., et al. (2021). Inhibiting with-no-lysine kinases enhances K<sup>+</sup>/Cl<sup>-</sup> cotransporter 2 activity and limits status epilepticus. *Brain* 144, 950–963. doi: 10.1093/brain/awab343
- Li, H., Khirug, S., Cai, C., Ludwig, A., Blaesse, P., Kolikova, J., et al. (2007). KCC2 interacts with the dendritic cytoskeleton to promote spine development. *Neuron* 56, 1019–1033. doi: 10.1016/j.neuron.2007.10.039
- Llano, O., Smirnov, S., Soni, S., Golubtsov, A., Guillemain, I., Hotulainen, P., et al. (2015). KCC2 regulates actin dynamics in dendritic spines via interaction with  $\beta$ -PIX. *J. Cell Biol.* 209, 671–686. doi: 10.1083/jcb.201411008
- Ludwig, A., Rivera, C., and Uvarov, P. (2017). A noninvasive optical approach for assessing chloride extrusion activity of the K-Cl cotransporter KCC2 in neuronal cells. *BMC Neurosci.* 18, 1–15. doi: 10.1186/s12868-017-0336-5
- Ludwig, A., Uvarov, P., Soni, S., Thomas-Crusells, J., Airaksinen, M. S., and Rivera, C. (2011). Early growth response 4 mediates BDNF induction of potassium chloride cotransporter 2 transcription. *J. Neurosci.* 31, 644–649. doi: 10.1523/JNEUROSCI.2006-10.2011
- McMoneagle, E., Zhou, J., Zhang, S., Huang, W., Josiah, S. S., Ding, K., et al. (2024). Neuronal K<sup>+</sup>-Cl<sup>-</sup> cotransporter KCC2 as a promising drug target for epilepsy treatment. *Acta Pharmacol. Sin.* 45, 1–22. doi: 10.1038/s41401-023-01149-9
- Mercado, A., Broumand, V., Zandi-Nejad, K., Enck, A. H., and Mount, D. B. (2006). A C-terminal domain in KCC2 confers constitutive K<sup>+</sup>-Cl<sup>-</sup> cotransport. *J. Biol. Chem.* 281, 1016–1026. doi: 10.1074/jbc.M509972200
- Moore, Y. E., Conway, L. C., Wobst, H. J., Brandon, N. J., Deeb, T. Z., and Moss, S. J. (2019). Developmental regulation of KCC2 phosphorylation has long-term impacts on cognitive function. *Front. Mol. Neurosci.* 12:173. doi: 10.3389/fnmol.2019.00173
- Moore, Y. E., Deeb, T. Z., Chadchankar, H., Brandon, N. J., and Moss, S. J. (2018). Potentiating KCC2 activity is sufficient to limit the onset and severity of seizures. *Proc. Natl. Acad. Sci. U. S. A.* 115, 10166–10171. doi: 10.1073/pnas.1810134115
- Pallud, J., Le Van Quyen, M., Bielle, F., Pellegrino, C., Varlet, P., Labussiere, M., et al. (2014). Cortical GABAergic excitation contributes to epileptic activities around human glioma. *Sci. Transl. Med.* 6:244ra89. doi: 10.1126/scitranslmed.3008065
- Pathak, H. R., Weissinger, F., Terunuma, M., Carlson, G. C., Hsu, F.-C., Moss, S. J., et al. (2007). Disrupted dentate granule cell chloride regulation enhances synaptic excitability during development of temporal lobe epilepsy. *J. Neurosci.* 27, 14012–14022. doi: 10.1523/JNEUROSCI.4390-07.2007
- Payne, J. A., Stevenson, T. J., and Donaldson, L. F. (1996). Molecular characterization of a putative K-Cl cotransporter in rat brain. *J. Biol. Chem.* 271, 16245–16252. doi: 10.1074/jbc.271.27.16245
- Pressey, J. C., Mahadevan, V., Khademullah, C. S., Dargaei, Z., Chevrier, J., Ye, W., et al. (2017). A kainate receptor subunit promotes the recycling of the neuron-specific K<sup>+</sup>-Cl<sup>-</sup> co-transporter KCC2 in hippocampal neurons. *J. Biol. Chem.* 292, 6190–6201. doi: 10.1074/jbc.M116.767236
- Puskarjov, M., Ahmad, F., Kaila, K., and Blaesse, P. (2012). Activity-dependent cleavage of the K-Cl cotransporter KCC2 mediated by calcium-activated protease calpain. *J. Neurosci.* 32, 11356–11364. doi: 10.1523/JNEUROSCI.6265-11.2012
- Puskarjov, M., Seja, P., Heron, S. E., Williams, T. C., Ahmad, F., Iona, X., et al. (2014). A variant of KCC2 from patients with febrile seizures impairs neuronal Cl<sup>-</sup> extrusion and dendritic spine formation. *EMBO Rep.* 15, 723–729. doi: 10.1002/embr.201438749
- Radulovic, T., Rajaram, E., Ebberts, L., Pagella, S., Winkhofer, M., Kopp-Scheinflug, C., et al. (2023). Serine 937 phosphorylation enhances KCC2 activity and strengthens synaptic inhibition. *Sci. Rep.* 13, 1–14. doi: 10.1038/s41598-023-48884-x



- Rinehart, J., Maksimova, Y. D., Tanis, J. E., Stone, K. L., Hodson, C. A., Zhang, J., et al. (2009). Sites of regulated phosphorylation that control K-cl cotransporter activity. *Cell* 138, 525–536. doi: 10.1016/j.cell.2009.05.031
- Rivera, C., Voipio, J., Payne, J. A., Ruusuvoori, E., Lahtinen, H., Lamsa, K., et al. (1999). The K+/cl- co-transporter KCC2 renders GABA hyperpolarizing during neuronal maturation. *Nature* 397, 251–255. doi: 10.1038/16697
- Saito, T., Ishii, A., Sugai, K., Sasaki, M., and Hirose, S. (2017). A de novo missense mutation in SLC12A5 found in a compound heterozygote patient with epilepsy of infancy with migrating focal seizures. *Clin. Genet.* 92, 654–658. doi: 10.1111/cge.13049
- Saitsu, H., Watanabe, M., Akita, T., Ohba, C., Sugai, K., Ong, W. P., et al. (2016). Impaired neuronal KCC2 function by biallelic SLC12A5 mutations in migrating focal seizures and severe developmental delay. *Sci. Rep.* 6, 1–12. doi: 10.1038/srep30072
- Sawant-Pokam, P. A., Vail, T. J., Metcalf, C. S., Maguire, J. L., McKean, T. O., McKean, N. O., et al. (2020). Preventing neuronal edema increases network excitability after traumatic brain injury. *J. Clin. Invest.* 130, 6005–6020. doi: 10.1172/JCI134793
- Stöberg, T., McTague, A., Ruiz, A. J., Hirata, H., Zhen, J., Long, P., et al. (2015). Mutations in SLC12A5 in epilepsy of infancy with migrating focal seizures. *Nat. Commun.* 6:8038. doi: 10.1038/ncomms9038
- Tang, B. L. (2016). K+-cl- co-transporter 2 (KCC2)—a membrane trafficking perspective. *Mol. Membr. Biol.* 33, 100–110. Taylor and Francis Ltd. doi: 10.1080/09687688.2017.1393566
- Tang, B. L. (2020). The expanding therapeutic potential of neuronal KCC2. *Cells* 9, 1–15. doi: 10.3390/cells9010240
- Tarentino, A. L., and Plummer, T. H. (1994). [4] enzymatic deglycosylation of asparagine-linked glycans: purification, properties, and specificity of oligosaccharide-cleaving enzymes from *Flavobacterium meningosepticum*. *Methods Enzymol.* 230, 44–57. doi: 10.1016/0076-6879(94)30006-2
- Trombetta, E. S., and Parodi, A. J. (2003). Quality control and protein folding in the secretory pathway. *Annu. Rev. Cell Dev. Biol.* 19, 649–676. doi: 10.1146/ANNUREV.CELLBIO.19.110701.153949
- Uvarov, P., Ludwig, A., Markkanen, M., Soni, S., Hübner, C., Rivera, C., et al. (2009). Coexpression and heteromerization of two neuronal K-cl cotransporter isoforms in neonatal brain. *J. Biol. Chem.* 284, 13696–13704. doi: 10.1074/jbc.M807366200
- Wan, L., Ren, L., Chen, L., Wang, G., Liu, X., Wang, B. H., et al. (2018). M-Calpain activation facilitates seizure induced KCC2 down regulation. *Front. Mol. Neurosci.* 11:287. doi: 10.3389/fnmol.2018.00287
- Watanabe, M., Wake, H., Moorhouse, A. J., and Nabekura, J. (2009). Clustering of neuronal K -Cl- cotransporters in lipid rafts by tyrosine phosphorylation. *J Biol Chem.* 284, 27980–27988. doi: 10.1074/jbc.M109.043620
- Weber, M., Hartmann, A.-M., Beyer, T., Ripperger, A., and Nothwang, H. G. (2014). A novel regulatory locus of phosphorylation in the C terminus of the potassium chloride cotransporter KCC2 that interferes with N-ethylmaleimide or staurosporine-mediated activation. *J. Biol. Chem.* 289, 18668–18679. doi: 10.1074/jbc.M114.567834
- Weilinger, N. L., Wicki-Stordeur, L. E., Groten, C. J., LeDue, J. M., Kahle, K. T., and MacVicar, B. A. (2022). KCC2 drives chloride microdomain formation in dendritic blebbing. *Cell Rep.* 41:111556. doi: 10.1016/J.CELREP.2022.111556
- Williams, J. R., Sharp, J. W., Kumari, V. G., Wilson, M., and Payne, J. A. (1999). The neuron-specific K-cl cotransporter, KCC2. *J. Biol. Chem.* 274, 12656–12664. doi: 10.1074/jbc.274.18.12656
- Xie, Y., Chang, S., Zhao, C., Wang, F., Liu, S., Wang, J., et al. (2020). Structures and an activation mechanism of human potassium-chloride cotransporters. *Advances* 6:eabc5883. doi: 10.1126/SCIADV.ABC5883
- Zhang, S., Zhou, J., Zhang, Y., Liu, T., Friedel, P., Zhuo, W., et al. (2021). The structural basis of function and regulation of neuronal cotransporters NKCC1 and KCC2. *Commun. Biol.* 4, 1–15. doi: 10.1038/s42003-021-01750-w
- Zhao, B., Wong, A. Y. C., Murshid, A., Bowie, D., Presley, J. F., and Bedford, F. K. (2008). Identification of a novel di-leucine motif mediating K(+)/cl(-) cotransporter KCC2 constitutive endocytosis. *Cell. Signal.* 20, 1769–1779. doi: 10.1016/j.cellsig.2008.06.011
- Zhou, H.-Y., Chen, S.-R., Byun, H. S., Chen, H., Li, L., Han, H.-D., et al. (2012). N-methyl-d-aspartate receptor- and calpain-mediated proteolytic cleavage of K+-cl- cotransporter-2 impairs spinal chloride homeostasis in neuropathic pain. *J. Biol. Chem.* 287, 33853–33864. doi: 10.1074/jbc.M112.395830